Weighted DC Virtual Generator Control Scheme for Interlinking Converters in DC Microgrids

Carlos Gómez-Aleixandre, *Member, IEEE*, Ángel Navarro-Rodríguez, *Member, IEEE*, Marius Langwasser, *Member, IEEE*, Pablo García, *Senior Member, IEEE*, and Marco Liserre, *Fellow, IEEE*

***Abstract*—This article proposes a new control strategy for power electronic converters interfacing two dc networks. The proposed control, based on a modification of the dc virtual generator concept, has grid-forming capability in both sides of the converter simultaneously without intermediate energy storage device. Departing from the dc virtual generator control concept, capable of controlling voltage in one of the converter sides while withdrawing the power from the other side, an adaptation is done to make it reversible. A priority weight is assigned to each side voltage control. A weight calculation method, proportional to the voltage deviation from its rated value, is proposed. This weight calculation strategy makes the control system to contribute to the side most in need (using voltage deviation with respect to rated value as an indicator of the neediness). The interlinking converter with the proposed weighted strategy is capable of stable work in grid-forming mode at both sides simultaneously, just requiring a grid-feeding converter with P/V droop to be connected in either side. No control architecture was found in the literature with this capability for dc–dc interlinking converters. The theoretical discussion has been supported with small-signal analysis and hardware-in-the-loop validation.**

***Index Terms*—DC-microgrids, grid-forming control, voltage control, dc virtual generator (DCVG).**

Manuscript received 27 February 2023; revised 27 June 2023 and 3 September 2023; accepted 26 September 2023. This work was supported in part by the Predoctoral Grants Program FPU for the Formation in University Teaching of Spain MECD under Grant FPU16/05313, in part by the Spanish Ministry of Science and Innovation and Ministry of Universities under Project MCINN-22-TED2021-129796B-C21 and Project MU-21-UP2021-030 47095823Q, in part by the Asturian Foundation for the Scientific and Technical Research (FICYT) under Project SV-PA-21-AYUD/2021/57546, and in part by the German Federal Ministry of Education and Research (BMBF) within the Kopernikus Project ENSURE "New ENergy grid StructURes for the German Energiewende" under Grant 03SFK1I0-2. *(Corresponding author: Carlos Gómez-Aleixandre.)*

Carlos Gómez-Aleixandre, Ángel Navarro-Rodríguez, and Pablo García are with the Department of Electrical, Electronics, Systems and Computers Engineering, LEMUR Group, University of Oviedo, 33204 Gijón, Spain (e-mail: gomeztcarlos@uniovi.es; navarroangel@uniovi.es; garciafpablo@uniovi.es).

Marius Langwasser and Marco Liserre are with the Chair of Power Electronics, Kiel University, 24118 Kiel, Germany (e-mail: mlan@tf.uni-kiel.de; ml@tf.uni-kiel.de).

Color versions of one or more figures in this article are available at https://doi.org/10.1109/TIE.2023.3323700.

Digital Object Identifier 10.1109/TIE.2023.3323700

I. Introduction

THE increasing importance of distributed energy resources (DERs) interfaced by power electronic converters (PECs) has led to the appearance of microgrids [1]. Although ac was traditionally more used, the benefits of dc has caused a gradual move toward dc distribution. These benefits include the easiness of integration of intermittent DER due to renewable sources (which normally requires extra dc–ac conversion stages in ac microgrids) and the reduced losses, due to the absence of reactive current flow, skin effect, and the reduced number of conversion stages [2], [3], [4], [5].

Despite of their advantages, microgrids present some challenges, such as their reduced inertia [6], [7], due to the substitution of rotating generators directly connected to the grid with PEC interfaced elements or the significant presence of renewable energy sources, which are often controlled to produce the maximum available power. This led to the appearance of the virtual generator concept [8], emulating the inertial characteristic of the rotating machines with the control strategy.

Interlinking converters play a key role to enhance reliability. Interlinking dc–dc converters can be used for connecting more than one dc microgrid to increase stability by having the capacity of exchanging power [4] or to have different voltage levels in the same microgrid [5]. These interlinking converters can also contribute to voltage regulation. A deep review of the capability to contribute to voltage regulation in both sides of the interlinking converters depending on the control architecture is presented in [9], distinguishing between grid-supporting and grid-forming capabilities for the converter. In [9] and [10], converters are considered to have grid-forming capability if they behave as a voltage source. This is a change in the traditional naming of droop-controlled converters as grid-supporting units regardless they were current-source or voltage source-based [11]. As stated in [10], this previous classification is less useful since it is not based on a fundamental difference between the sources. The definition used in [9] and [10] will be used throughout this article, especially for highlighting the necessity of at least one grid-forming converter in each network.

Some solutions can be found in the literature for dc–ac converters interfacing an ac microgrid with a dc-link capacitor at the output of a converter connected to an energy source. This is done with a droop relating ac and dc voltage (V_g/V_{dc} droop) [12] or a dual droop, adding a dc voltage term to ac droop equations [13].

However, apart from being dc–ac converter cases, grid-forming capability is only supported in one output, having dual grid-supporting and single grid-forming capability [9].

Similarly, previous research is reported both for ac–dc [14] and dc–dc [15] interlinking converters that consider additional grid-forming units in either side. In the event an interconnected network losses its grid-forming unit, the interlinking converter will give voltage control capability to that network by power transfer from the grid-forming unit in the other side. This can be done without control scheme switching and operation mode detection. However, this method needs a grid-forming unit in one of the networks to have a reversible grid-forming capability with seamless transition.

The strategy proposed in [8] for ac–dc converters has dual grid-forming capability, i.e., the capability of controlling voltage in both sides of the converter to reasonable levels, just requiring some type of grid-feeding converter with grid-supporting strategies in one of the networks. No control architecture has been found in the literature with dual grid-forming capability for dc–dc converters [9].

This article proposes a new control strategy based on the well-known dc virtual generator (DCVG) concept [8], [16], [17]. From the DCVG scheme, an adaptation is done to make the control reversible, i.e., to use the same voltage control scheme for controlling the voltage in either side. The proposed modification considers a weighted approach, in which a priority can be given to each side. By considering a weight calculation strategy proportional to the deviation with respect to the rated voltage, dual grid-forming capability is achieved: the proposed method provides grid-forming capability to both outputs at the same time. It only requires a grid-feeding converter with a P/V droop in any side to keep the voltage in both grids at reasonable levels and without requiring communication between the converters. As compared to the DCVG control, the proposal is able to: 1) adapt to change in configurations of the network, for example, automatically adapt to islanded mode (reversible grid-forming capability) and 2) provide grid-forming capability to both outputs simultaneously, just requiring an appropriate grid-supporting element in any side (dual grid-forming capability).

The rest of this article is organized as follows. Section II presents the grid used for this study. Section III describes the proposed control, whose stability is analyzed in Section IV. Section V explains the case study, presenting the different grid configurations that are considered for the analysis. Section VI presents the results obtained with hardware-in-the-loop (HIL) for the validation of the proposed control. Finally, Section VII concludes this article.

II. Proposed DC Microgrid Topology

The proposed study uses a subgrid from the one explained in [18]. The schematic representation is shown in Fig. 1. As it can be seen, it includes a 375 Vdc bus and a 48 Vdc network connected to it using an interlinking PEC. The 48 Vdc network will be referred as converter side 1, while the 375 Vdc bus connection is named side 2.

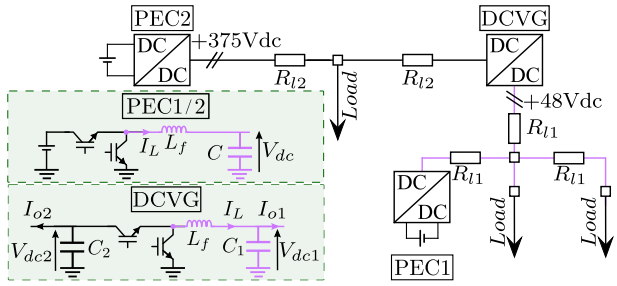

Fig. 1. Grid used for HIL validation. Shadowed boxes show filter and converter configuration and control variables for each subgrid converter (PEC1 and PEC2) and for interlinking converter (DCVG). All converters have a synchronous buck configuration, being the inductor filter in the low voltage side (V_{dc1} in the case of the DCVG).

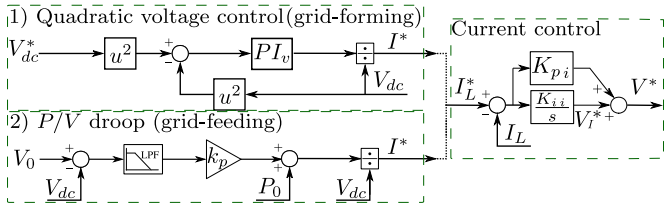

Fig. 2. PEC1 and PEC2 control diagram, showing both grid-forming (with quadratic voltage control [19]) and grid-feeding alternatives.

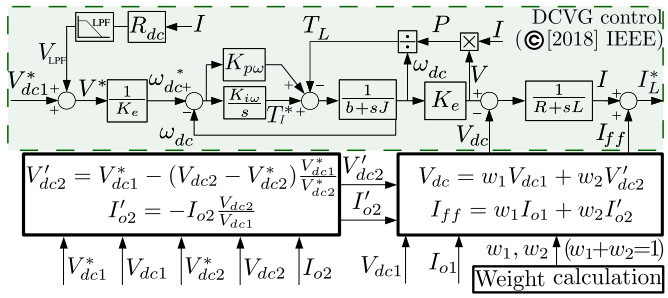

Fig. 3. WDCVG control. Shadowed box shows the conventional DCVG strategy [8].

The converter with the proposed control strategy is labeled as DCVG, meanwhile in each of the dc networks there is another dc–dc converter contributing to voltage regulation. PEC2 represents a connection to the mains, simplified here as a dc–dc converter, always operating as a grid-forming unit. PEC1 can represent any DER operating in grid forming or grid feeding with P/V droop. PEC1 and PEC2 control is shown in Fig. 2, meanwhile interlinking control (marked as DCVG in Fig. 1) is explained in the following section.

III. Proposed Control

A. Weighted Dc Virtual Generator (WDCVG)

The proposed control, shown in Fig. 3, is obtained from the conventional DCVG scheme [8], [16], [17], with some modifications in order to be able to control the voltage in either side of the converter (V_{dc1} or V_{dc2}) when the DCVG is acting as an interlinking converter. Current control, not included to keep the

figure readable, has the same structure as shown in Fig. 2 for PEC1 and PEC2.

The proposed control is based on combining a voltage control strategy focused on each side of the converter by applying a weighted average. This is shown in (1a) and (1b), being w_1 and w_2 the weight corresponding to sides 1 and 2, respectively, with $0 \leq w_x \leq 1$ and $w_1 + w_2 = 1$. V_{dc} and I_{ff} represent the averaged voltage and feedforward current, obtained from output voltage and current in side 1 (V_{dc1}, I_{o1}) and side 2, but referring the latter ones to side 1 (V'_{dc2}, I_{o2}')

$$V_{\text{dc}} = w_1 V_{\text{dc1}} + w_2 V'_{\text{dc2}} \tag{1a}$$

$$I_{\text{ff}} = w_1 I_{o1} + w_2 I'_{o2}. \tag{1b}$$

For adapting the voltage in side 2 (V_{dc2}) to side 1 (V'_{dc2}) a change in voltage base is applied, but also changing the sign of voltage deviation. For example, $V_{\text{dc2}} = (1 + \Delta V_{\text{dc2}})V^*_{\text{dc2}}$ will be transformed into $V'_{\text{dc2}} = (1 - \Delta V_{\text{dc2}})V^*_{\text{dc1}}$, being ΔV_{dc2} the per unit voltage deviation in side 2. The change in sign of the voltage deviation is due to the fact that for increasing the voltage in one of the sides, the required power has opposite direction to the one required for increasing the voltage in the other side. The required transformation is shown in the following equation:

$$V'_{\text{dc2}} = (1 - \Delta V_{\text{dc2}})V^*_{\text{dc1}} = V^*_{\text{dc1}} - (V_{\text{dc2}} - V^*_{\text{dc2}})\frac{V^*_{\text{dc1}}}{V^*_{\text{dc2}}}. \tag{2}$$

For adapting side 2 current to side 1, I'_{o2} is calculated as the current in side 1 output which will produce the same power output I_{o2} produces in side 2. This is done by multiplying the output current I_{o2} by $V_{\text{dc2}}/V_{\text{dc1}}$ and changing its sign. The corresponding expression is shown in the following equation:

$$I'_{o2} = -I_{o2}\frac{V_{\text{dc2}}}{V_{\text{dc1}}}. \tag{3}$$

Weights w_1 and w_2 can be fixed according to different criteria. An upper control level could set it depending on the grid situation. For example, if one of the grids has another converter with grid-forming capability, the weight corresponding to that side can be set to 0. By doing this, the DCVG will only control the voltage in the other side, acting as a grid-forming unit for that network. If both grids have grid-forming units, the weights can be set dynamically, taking into account which grid is closer to reach any saturation limit or has more critical loads, lower DER participation, or lower inertia.

Another option is to do a complete switch in the side whose voltage is being controlled attending to some voltage threshold. For example, initially w_1 can be set to 1 (and $w_2 = 0$) meanwhile voltage in side 2 is within some range. If voltage in side 2 exits the predefined range, the interlinking control starts controlling that output ($w_1 = 0$ and $w_2 = 1$). This is similar to the voltage margin control found in [20].

B. Proportionally Weighted DCVG (PWDCVG)

This article proposes a weight calculation strategy proportional to the voltage deviation with respect to the rated value in each converter side. This is shown in (4), where ΔV_{dc1} and ΔV_{dc2} are each side per unit voltage deviation and w_x is the weight of side 1 or 2

$$w_x = \frac{\frac{|V_{\text{dc}x} - V^*_{\text{dc}x}|}{V^*_{\text{dc}x}}}{\frac{|V_{\text{dc1}} - V^*_{\text{dc1}}|}{V^*_{\text{dc1}}} + \frac{|V_{\text{dc2}} - V^*_{\text{dc2}}|}{V^*_{\text{dc2}}}} = \frac{|\Delta V_{\text{dc}x}|}{|\Delta V_{\text{dc1}}| + |\Delta V_{\text{dc2}}|}. \tag{4}$$

By doing this, the control focuses more on the side, which is further away from nominal voltage, without requiring any upper layer control to infer it from the grid conditions. Additionally, the proposed system avoids any sharp transition between the side whose voltage is being controlled produced by sudden changes of weights w_1 and w_2. Instead, a smooth and continuous change in the priority for each side is achieved, resulting in smoother transients.

By following this strategy, equal per unit voltage deviation is achieved in both sides of the converter in steady state, as it will be shown in Section VI. This can be proven by finding the value, which makes V_{dc} in (1a) equal to V^*_{dc1}, because due to the virtual resistance decoupling, equilibrium point fulfills $V_{\text{dc}} = V^*_{\text{dc1}}$.

Substituting V_{dc} by V^*_{dc1} in (1a), (5) is obtained. V_{dc1} and V'_{dc2} are expressed in terms of V^*_{dc1}, taking into account V'_{dc2} is obtained by changing the sign of the per unit voltage deviation measured in side 2 as shown in (2)

$$V^*_{\text{dc1}} = w_1(1 + \Delta V_{\text{dc1}})V^*_{\text{dc1}} + w_2(1 - \Delta V_{\text{dc2}})V^*_{\text{dc1}}. \tag{5}$$

Simplifying V^*_{dc1} and with the cancelation of all terms independent of ΔV_{dc1} and ΔV_{dc2} due to the fact that $w_1 + w_2 = 1$, the expression in (6) is obtained

$$w_1 \Delta V_{\text{dc1}} = w_2 \Delta V_{\text{dc2}}. \tag{6}$$

Finally, w_1 and w_2 can be substituted by the formula in (4). After simplifying the denominator, (7) is obtained. The only solution for this equation is $\Delta V_{\text{dc1}} = \Delta V_{\text{dc2}}$, obtaining, in steady state, $w_1 = w_2 = 0.5$

$$|\Delta V_{\text{dc1}}|\Delta V_{\text{dc1}} = |\Delta V_{\text{dc2}}|\Delta V_{\text{dc2}}. \tag{7}$$

As a final remark about the proposed mechanism, it has to be highlighted that with the weighted strategy the interlinking converter can behave as a grid-forming converter for both sides simultaneously, just requiring an additional grid-feeding unit with P/V droop in either side. This will be demonstrated in Section VI.

IV. Stability Analysis

The stability of the proposed control is analyzed by using the state-space model. The state-space matrix, together with the input and state variables, are shown in (8) to (13). The matrices and terms in red are time varying. Thus, linearization is required to obtain the small-signal model for the analysis. I_{o1} and I_{o2} were considered as system inputs. However, this will generally not be the case when looking to the complete system. One or both sides of the converter will normally be connected to a voltage source through a line impedance, which provides the required power. In that case, the corresponding input I_{ox} should be replaced by $\frac{V_{\text{dc}x} - V_{sx}}{R_x}$, thus affecting both A and B matrices

$$\dot{x} = \left[A_1 \mid A_2\right] x + Bu \tag{8}$$

$$x = [\omega_{\text{dc}} \;\; I \;\; T_I^* \;\; V_{\text{LPF}} \;\; V_I^* \;\; V_{\text{dc1}} \;\; V_{\text{dc2}} \;\; I_L]^T \tag{9}$$

$$u = [V_{\text{dc1}}^* \;\; I_{o1} \;\; I_{o2}]^T \tag{10}$$

$$A_1 = \begin{bmatrix} -\frac{K_{\text{pw}}+b}{J} & -\frac{K_e}{J} & \frac{1}{J} & \frac{K_{\text{pw}}}{JK_e} \\ \frac{K_e}{L} & -\frac{R}{L} & 0 & 0 \\ -K_{\text{iw}} & 0 & 0 & \frac{K_{\text{iw}}}{K_e} \\ 0 & R\omega_{\text{LPF}} & 0 & -\omega_{\text{LPF}} \\ 0 & K_{ii} & 0 & 0 \\ 0 & 0 & 0 & 0 \\ 0 & -\frac{K_{pi} i_L}{C_2 V_{\text{dc2}}} & 0 & 0 \\ 0 & \frac{K_{pi}}{L_f} & 0 & 0 \end{bmatrix} \tag{11}$$

$$A_2 = \begin{bmatrix} 0 & 0 & 0 & 0 \\ 0 & -\frac{w_1}{L} & \frac{V_{\text{dc1}}^* w_2}{L V_{\text{dc2}}^*} & 0 \\ 0 & 0 & 0 & 0 \\ 0 & 0 & 0 & 0 \\ 0 & 0 & 0 & -K_{ii} \\ 0 & 0 & 0 & \frac{1}{C_1} \\ -\frac{i_L}{C_2 V_{\text{dc2}}} & -\frac{i_L}{C_2 V_{\text{dc2}}} & 0 & \frac{K_{pi} i_L}{C_2 V_{\text{dc2}}} \\ \frac{1}{L_f} & 0 & 0 & -\frac{K_{pi}}{L_f} \end{bmatrix} \tag{12}$$

$$B = \begin{bmatrix} \frac{K_{\text{pw}}}{JK_e} & 0 & 0 \\ -\frac{2w_2}{L} & 0 & 0 \\ \frac{K_{iw}}{K_e} & 0 & 0 \\ 0 & 0 & 0 \\ 0 & K_{ii} w_1 & -\frac{K_{ii} V_{\text{dc2}} w_2}{V_{\text{dc1}}} \\ 0 & -\frac{1}{C_1} & 0 \\ 0 & -\frac{K_{pi} i_L w_1}{C_2 V_{\text{dc2}}} & \frac{K_{pi} i_L w_2 - V_{\text{dc1}}}{C_2 V_{\text{dc1}}} \\ 0 & \frac{K_{pi} w_1}{L_f} & -\frac{K_{pi} V_{\text{dc2}} w_2}{L_f V_{\text{dc1}}} \end{bmatrix}. \tag{13}$$

The proposed PWDCVG is compared with the traditional DCVG scheme applied to side 1 ($w_1 = 1$) or to side 2 ($w_2 = 1$). Since $w_1 = w_2 = 0.5$ in steady state for PWDCVG (as shown in Section III-B) the application of the WDCVG with a fixed value of 0.5 for the weights is also considered. The system parameters are shown in Table I.

To prove the reversible and simultaneous grid-forming capability of the proposed control, two different scenarios are considered. Case $V_{s1} - I_{o2}$: side 1 is connected to a voltage source that provides the power demand by a current source in side 2. Case $I_{o1} - V_{s2}$ is the opposite scenario. The eigenvalues for both scenarios are shown in Fig. 4, where it can be seen that only PWDCVG and $w_x = 0.5$ are stable in both scenarios, with $w_2 = 0$ having an eigenvalue at the origin and $w_1 = 0$ at the right half-plane in the case where the voltage source is in the opposite side of the one with weight equal to 0.

TABLE I
SYSTEM PARAMETERS

Grid parameters	Values
Side 1 voltage: V_{dc1}^*	48 Vdc
Side 1 line resistance: R_{l1}	6.9 mΩ
Side 2 voltage: V_{dc2}^*	375 Vdc
Side 2 line resistance: R_{l2}	105.5 mΩ
PEC1 parameters	**Values**
Filter inductance, capacitance: L_f, C_f	0.73 mH, 5 mF
Current regulator bandwidth: BW_i	500 Hz
Voltage regulator bandwidth: BW_v	50 Hz
P/V droop constant: k_{pv}	8.33 kW/V
PEC2 parameters	**Values**
Filter inductance, capacitance: L_f, C_f	2.5 mH, 5.04 mF
Current regulator bandwidth: BW_i	500 Hz
Voltage regulator bandwidth: BW_v	50 Hz
WDCVG parameters	**Values**
Nominal power: P_n	5 kW
Filter inductance: L_f	1.47 mH
Filter capacitance (side 1): C_f	5.04 mF
DC link capacitance (side 2): C_f	5 mF
Current regulator bandwidth: BW_i	500 Hz
Governor regulator bandwidth: BW_ω	50 Hz
Virtual inertia, damping: J_{dc}, b_{dc}	0.0002 kg·m^2, 0.003 N·m·s
Virtual inductance, resistance: L_{dc}, R_{dc}	0 H, 10 mΩ

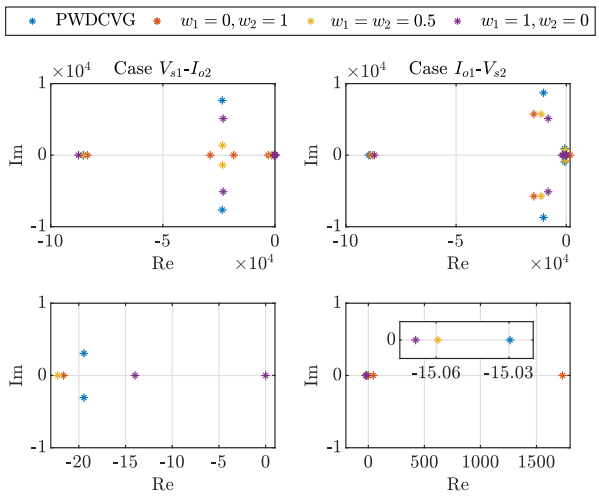

Fig. 4. Eigenvalues for PWDCVG and different values for w_1 and w_2. Left column: case $V_{s1} - I_{o2}$; right column: case $I_{o1} - V_{s2}$. Top row: the general view with all the eigenvalues; bottom row: a zoom to cover all the dominant eigenvalues. A zoom is presented in the bottom right figure to distinguish overlapping eigenvalues.

The step responses of the same cases for voltage outputs $V_{\text{dc}x}$ are shown in Fig. 5, where a variation of a step of magnitude $0.1V_{\text{dc}x}^*$ and I_{nx} (nominal current in side x) is applied to the corresponding input. It can be seen that only PWDCVG and $w_x = 0.5$ are stable in all scenarios, but PWDCVG is faster and has less overshoot.

V. CASE STUDY

The microgrid used as the case study is shown in Fig. 1, with all the grid and converter parameters included in Table I. For checking the operation of the converter in different scenarios, transitions between different configuration modes of the microgrid are introduced by connecting/disconnecting PEC1 and PEC2 units. The different operation modes of the microgrid are shown in Table II.

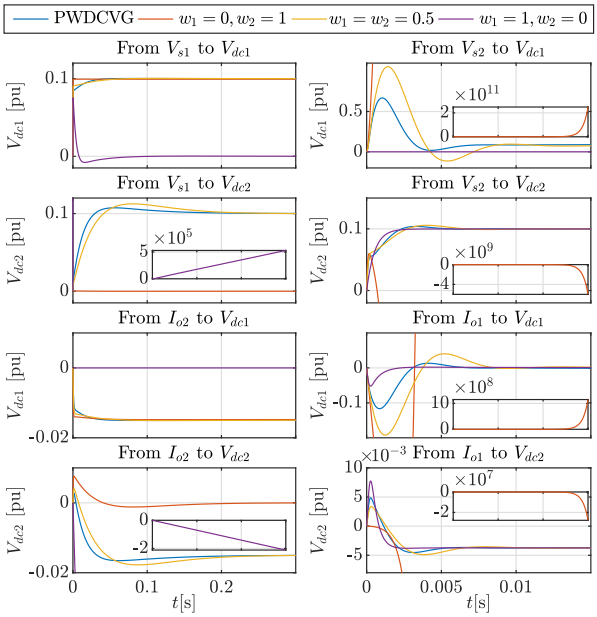

Fig. 5. Step response for PWDCVG and different values for w_1 and w_2. Left column: case $V_{s1} - I_{o2}$; right column: case $I_{o1} - V_{s2}$. First row: response of V_{dc1} to change in V_{sx}. Second row: response of V_{dc2} to change in V_{sx}. Third row: response of V_{dc1} to change in I_{ox}. Fourth row: response of V_{dc2} to change in I_{ox}. Unstable responses are shown in a small window in the corresponding plot.

TABLE II
DIFFERENT OPERATING MODES OF THE MICROGRID

Mode	PEC1	PEC2
A1	Grid-forming	Grid-forming
A2	Grid-feeding with P/V droop	Grid-forming
B1	Grid-forming	Off
B2	Grid-feeding with P/V droop	Off
C	Off	Grid-forming

Four different scenarios are considered. For the first three, PEC1 operates as grid-forming unit. Each of the 4 scenarios listed there correspond to one subsection in the same order they appear. So scenario 1 is presented in Subsection VI.A, scenario 2 is presented in VI.B and so on.

1) Step in weights setting different values to show how sending weight references can change the way the WDCVG contributes to both networks. Converters in mode A1.
2) The strategy based on voltage margin control is followed. Initially, w_1 is fixed to 1 ($w_2 = 0$), making the WDCVG only contribute to control in side 1 (48 Vdc network). Starting in mode A1, there is a transition to mode B1, leading to an uncontrolled voltage in side 2 (375 Vdc network). When the voltage in that network goes outside some limits, w_1 is changed to 0 and w_2 to 1 so that the WDCVG starts to control the voltage in side 2.
3) Proportionally WDCVG is used in the same scenario shown for voltage margin control case in order to compare both scenarios. A longer HIL simulation for proportionally WDCVG is also shown to demonstrate how transition between different scenarios affects the grid situation, with transitions between A1, B1, and C modes.

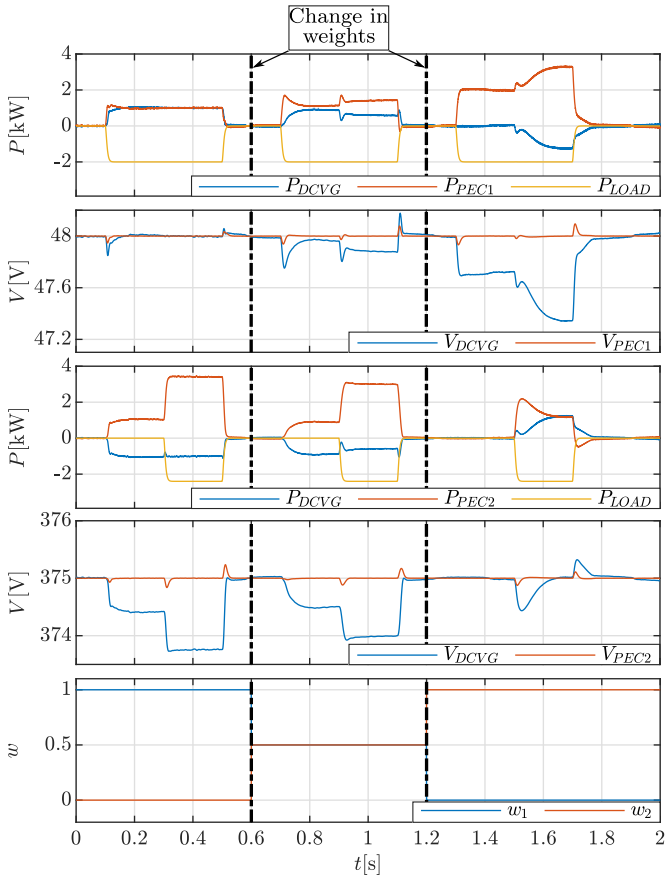

Fig. 6. HIL results for step changes in weights with converters in mode A1. Vertical lines indicate change in weight values. From top to bottom: power in side 1 (48 Vdc network); voltage in side 1; power in side 2 (375 Vdc network); voltage in side 2; each side weight value.

4) Apart from that, a HIL simulation equal to the last mentioned one is done but changing PEC1 to be a grid-feeding unit with droop control (transitions between A2, B2, and C modes).

VI. HIL RESULTS

The proposed control has been validated by using a HIL setup, composed of a Typhoon HIL404 platform and a TMS320F28335 TI control card. The HIL time step is 1 μs, the sampling time of the converters control is 100 μs and their switching frequency is 10 kHz. The data shown in this article have been captured with a rate of 10 kS/s.

A. Steps in Weights

The first scenario is done for the weighted DCVG generator working with different values of weights which are step-wise varied. The results are shown in Fig. 6. Power is expressed using active sign convention: positive for generation, negative for consumption.

The initial situation is with $w_1 = 1$ ($w_2 = 0$). Starting from no load, at $t = 0.1$ s a step of 2 kW in the power demanded by the load in 48 Vdc network. At $t = 0.3$ s, a step of 2.4 kW in the power demanded by the load in 375 Vdc network. At $t = 0.5$ s,

the power demanded by the loads in both networks is set back to 0 kW. w_1 (w_2) is changed to 0.5 (0.5) at $t = 0.6$ s and to 1 (0) at $t = 1.2$ s. After these two changes, the same steps in demand mentioned for $w_1 = 1$ are used.

When $w_1 = 1$ ($w_2 = 0$), the control is focusing only in the voltage control in 48 Vdc network. It can be seen that in that interval the control of the DCVG is not affected by the power changes in the other side ($t = 0.3$ s).

When $w_1 = w_2 = 0.5$ (after $t = 0.6$ s), the control is contributing in the same proportion to both sides. It can be seen that, in this case, the control reacts to power changes in both grids ($t = 0.7$ s and $t = 0.9$ s).

After the second vertical line, w_1 is set to 0 ($w_2 = 1$), having the opposite of the initial situation. The control is only focusing in the 375 Vdc network and not affected by power changes in the other network ($t = 1.3$ s)

B. Weighted DCVG With Voltage Margin Control

In order to check the capability of autonomous voltage control, when any one side is lacking a grid-forming converter, a weight calculation strategy similar to voltage margin control is studied. The weight of the DCVG is set to 1 in normal operation, thus focusing on voltage control in the 48 Vdc network. When the voltage in the 375 Vdc network goes outside a pre-set dead-band (370–380 Vdc in this case), the weight is changed to 0, switching to voltage control in the other side.

If the margin control strategy is applied to the weighted DCVG, the results shown in Fig. 7 are obtained. Starting in mode A1, with PEC1 and PEC2 operating as grid forming, load references in each side are changed. At $t = 0.1$ s, the load in the 48 Vdc network is set to -2 kW (demand) and changed to 3 kW (production) at $t = 0.7$ s. At $t = 0.3$ s, the load in the 375 Vdc network is set to -2.4 kW and changed to 1.6 kW at $t = 0.5$ s. It can be seen that load changes in the 375 Vdc network are totally absorbed by PEC2, since the DCVG converter is only focused in side 1 when the voltage in side 2 is within the limits.

After the vertical line, the only converter controlling the voltage in 375 Vdc network (PEC2) is disconnected. When the voltage goes out of the specified limits, the DCVG starts to control the voltage in that side, setting the dc voltage reference to 380 V. This allows the converter to be able to work in both directions. However, sudden changes in the control mode also causes fast voltage variation when there is no converter in voltage control in a given grid. It should also be remarked that, when similar conditions occur at the two sides, it would be difficult to select which one to give priority.

C. PWDCVG (With Grid-Forming Converters in Both Networks)

To solve the previous two problems, the proposed weight calculation strategy obtains each weight proportional to the voltage deviation with respect to the rated values in each converter side. In that way, the voltage deviation from the reference point is used as a measure of the neediness of each side and the priority is set proportional to it. This leads to weights within the range 0 to 1 and results in a smooth operation during grid situation changes.

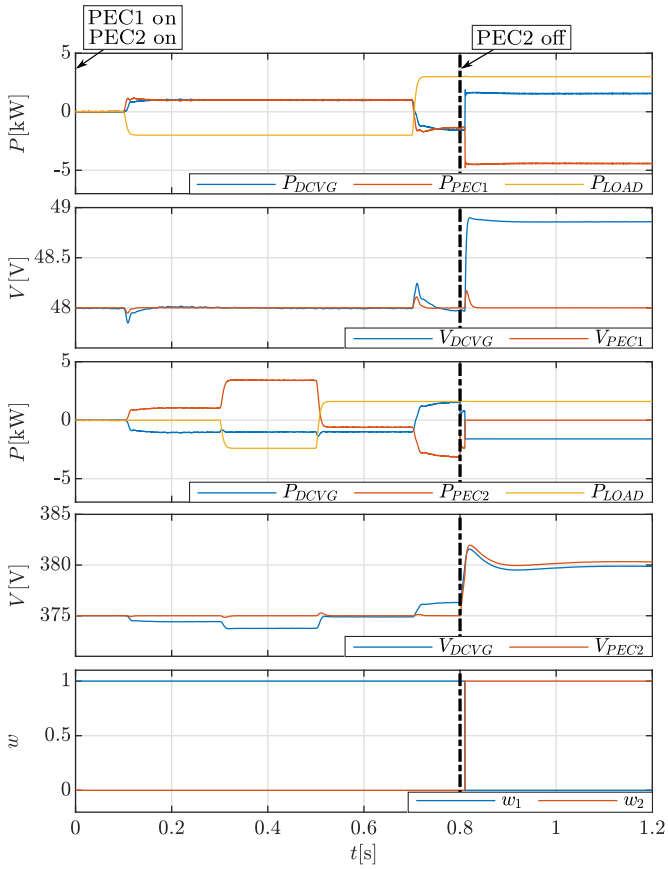

Fig. 7. HIL results for weighted DCVG with voltage margin control with PEC1 as grid forming. Vertical line indicates change from mode A1 to mode B1. From top to bottom: power in side 1 (48 Vdc network); voltage in side 1; power in side 2 (375 Vdc network); voltage in side 2; each side weight value.

This can be seen in Fig. 8, which is the same situation (configuration and load sequence) of Fig. 7 but with the explained weight calculation strategy. The proposed strategy reacts smoothly to PEC2 disconnection, reducing the rate of change of the voltage in the uncontrolled grid.

Fig. 9 shows a longer sequence of changes for a complete demonstration of the operation of the converter in different grid configurations. Starting in mode C (PEC1 off, PEC2 acting as grid forming), the sequence of changes is the following.

1) $t = 0.1$ s: load in 48 Vdc network is set to -2 kW (demand).
2) $t = 0.3$ s: load in 375 Vdc network is set to -2.4 kW (demand).
3) $t = 0.4$ s: PEC1 is connected, acting as grid forming, changing operating mode to A1.
4) $t = 0.5$ s: load in 375 Vdc network is set to 1.6 kW (production).
5) $t = 0.7$ s: load in 48 Vdc network is set to 3 kW (production).
6) $t = 0.8$ s: PEC2 is disconnected, changing operating mode to B1.
7) $t = 1.0$ s: load in 375 Vdc network is set to -2.4 kW (demand).

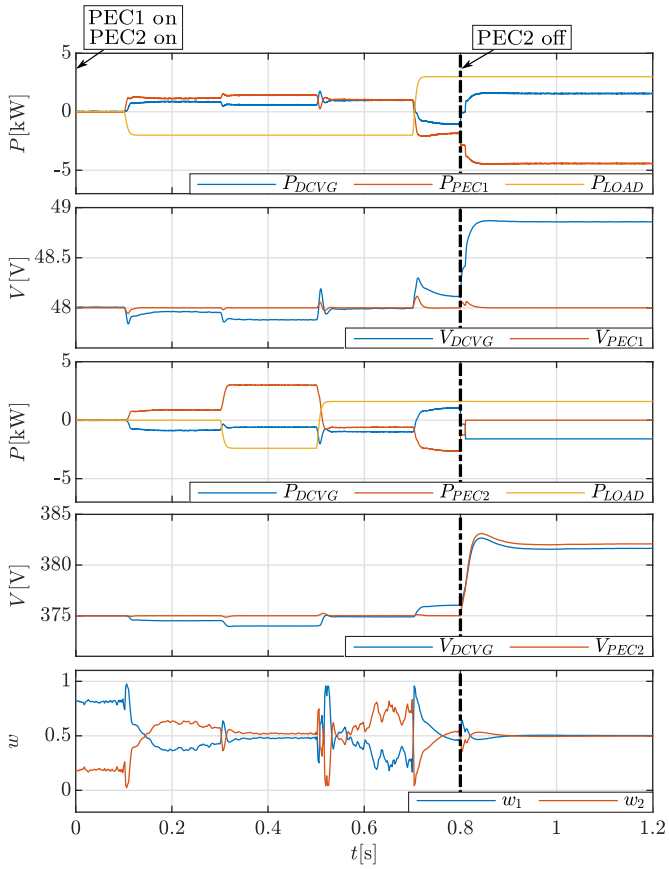

Fig. 8. HIL results for PWDCVG with PEC1 as grid forming. Vertical line indicates change from mode A1 to mode B1. From top to bottom: power in side 1 (48 Vdc network); voltage in side 1; power in side 2 (375 Vdc network); voltage in side 2; each side weight value.

8) $t = 1.4$ s: PEC2 is connected, acting as grid forming, changing operating mode to A1.
9) $t = 1.6$ s: PEC1 is disconnected, changing operating mode to C.

It can be seen that the control is able to act as grid-forming converter in any of the sides keeping the voltage stable in both sides, even if the other grid-forming converter in the corresponding network is disconnected. Apart from that, when both PEC1 and PEC2 are operating, the DCVG reacts to load changes in both sides, making it possible to each PEC to contribute to the load in the other network.

Current outputs are shown too, where it can be seen that the ripple in the current is not very significant. The ripple is higher in 375 Vdc network (side 2) because side 1 is the one with the *LC* filter (see Fig. 1).

Finally, a comparison in the per unit voltage at each side of the converter is shown. As it was demonstrated mathematically, it can be seen that, in steady state, the voltage deviation is equal in both sides. This means that it is able to reach a balanced situation in which both networks are in similar neediness as seen from both converter output voltages.

D. PWDCVG (With Grid Feeding)

The proportionally WDCVG has the capability of acting as grid forming in both networks at the same time, with no need of other grid-forming unit in either side. Only one converter acting as grid feeding with droop control is required for the proposed control to be able to control voltage in both sides at the same time.

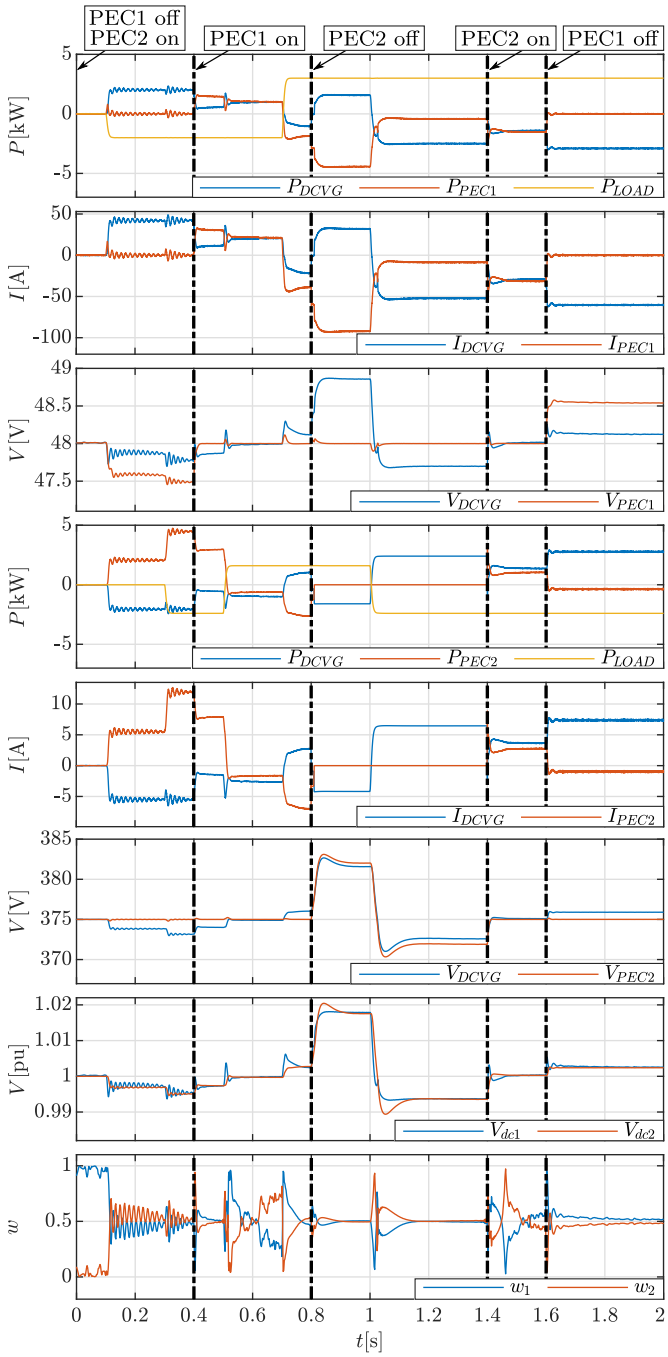

Fig. 9. HIL results for PWDCVG with PEC1 as grid forming. From top to bottom: power in side 1 (48 Vdc network); current in side 1; voltage in side 1; power in side 2 (375 Vdc network); current in side 2; voltage in side 2; per unit voltage in each side; each side weight value.

This is shown in Fig. 10, with exactly the same scenario shown in Fig. 9, but changing the grid-forming unit in 48 Vdc network by a grid-feeding unit with P/V droop. Thus, the sequence is the one presented before, but changing modes A1 and B1 for A2 and B2. It can be seen that even when the only grid-forming unit in

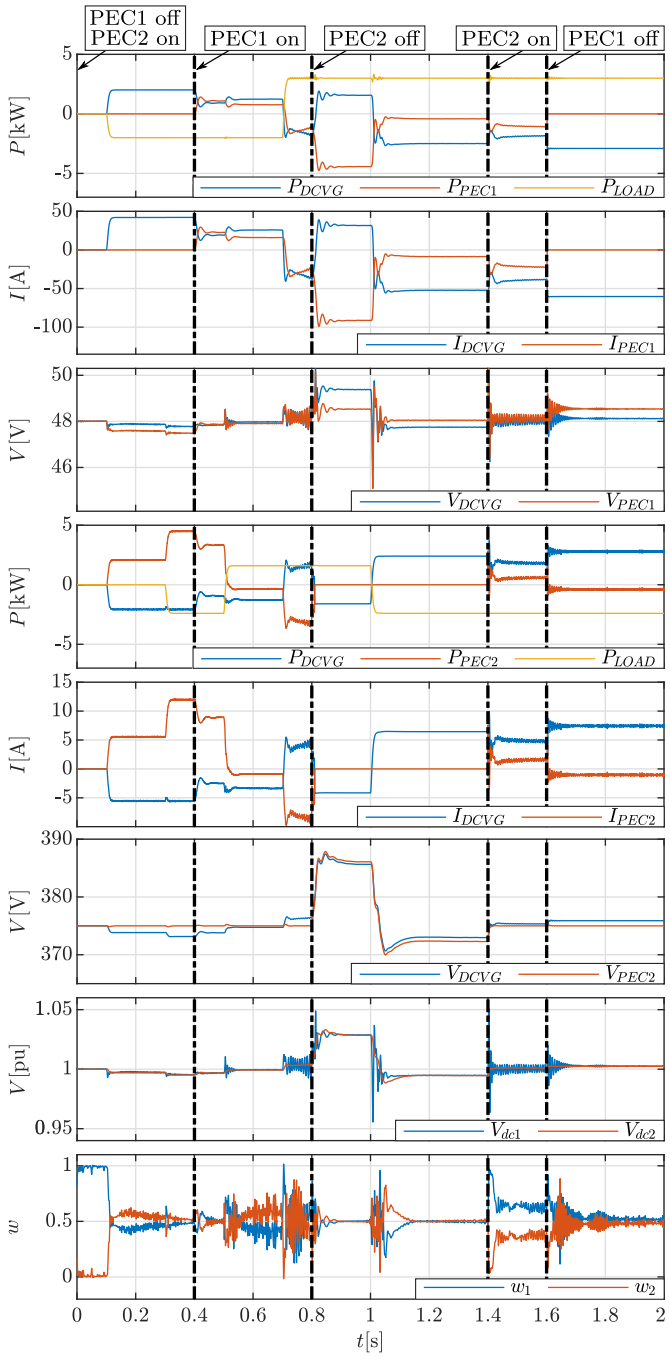

Fig. 10. HIL results for PWDCVG with PEC1 as grid feeding with P/V droop. From top to bottom: power in side 1 (48 Vdc network); current in side 1; voltage in side 1; power in side 2 (375 Vdc network); current in side 2; voltage in side 2; per unit voltage in each side; each side weight value.

the system apart from the DCVG interlinking converter (PEC2) is disconnected after the second vertical line, the interlinking converter is able to reach stable situation forming both grids at the same time.

In this case, the voltage deviation is higher than for the case with grid-forming units in both networks due to the P/V droop required for the grid-feeding unit to contribute. However, this situation will only happen due to contingencies and a secondary control can recover the voltage level. Besides that, voltage oscillations are more significant due to the lower capability of grid-feeding elements to contribute to voltage support.

VII. Conclusion

This article proposes a new control strategy based on a modification of the DCVG to adapt the control to make it able to control voltage in either side of the converter, providing grid-forming capability. A weight is given to each side so that the control focuses more on that side.

The proposed weighted DCVG is designed using weights proportional to the deviation of each converter side voltages from rated point. This makes the control to prioritize the grid, which is more in need. Small-signal analysis was performed to study the stability of the proposed method.

The performance was validated with Typhoon HIL404 platform. The results show the capability of the converter of operating in any scenario, provided that at least in one of the grids there is a converter providing the required power, either with grid-forming units or grid feeding with P/V droop. No control architecture was found in the literature with this capability for dc–dc interlinking converters. It was shown that, in steady state, the proposed control achieves the same voltage deviation in both sides, obtaining a good balance between the neediness of both.

References

[1] M. Ahmed, L. Meegahapola, A. Vahidnia, and M. Datta, "Stability and control aspects of microgrid architectures—A comprehensive review," *IEEE Access*, vol. 8, pp. 144730–144766, 2020, doi: 10.1109/ACCESS.2020.3014977.

[2] F. S. Al-Ismail, "DC microgrid planning, operation, and control: A comprehensive review," *IEEE Access*, vol. 9, pp. 36154–36172, 2021, doi: 10.1109/ACCESS.2021.3062840.

[3] S. Ullah, A. M. Haidar, P. Hoole, H. Zen, and T. Ahfock, "The current state of distributed renewable generation, challenges of interconnection and opportunities for energy conversion based DC microgrids," *J. Cleaner Prod.*, vol. 273, 2020, Art. no. 122777, doi: 10.1016/j.jclepro.2020.122777. [Online]. Available: https://www.sciencedirect.com/science/article/pii/S0959652620328225

[4] T. Dragičević, X. Lu, J. C. Vasquez, and J. M. Guerrero, "DC microgrids–part II: A review of power architectures, applications, and standardization issues," *IEEE Trans. Power Electron.*, vol. 31, no. 5, pp. 3528–3549, May 2016, doi: 10.1109/TPEL.2015.2464277.

[5] T. Dragičević, J. C. Vasquez, J. M. Guerrero, and D. Skrlec, "Advanced LVDC electrical power architectures and microgrids: A step toward a new generation of power distribution networks.," *IEEE Electrific. Mag.*, vol. 2, no. 1, pp. 54–65, Mar. 2014, doi: 10.1109/MELE.2013.2297033.

[6] P. Tielens and D. Van Hertem, "The relevance of inertia in power systems," *Renewable Sustain. Energy Rev.*, vol. 55, pp. 999–1009, Mar. 2016, doi: 10.1016/j.rser.2015.11.016.

[7] G. Delille, B. Francois, and G. Malarange, "Dynamic frequency control support by energy storage to reduce the impact of wind and solar generation on isolated power system's inertia," *IEEE Trans. Sustain. Energy*, vol. 3, no. 4, pp. 931–939, Oct. 2012, doi: 10.1109/TSTE.2012.2205025.

[8] A. Navarro-Rodríguez, P. García, C. Gómez-Aleixandre, and C. Blanco, "Cooperative primary control of a hybrid AC/DC microgrid based on AC/DC virtual generators," *IEEE Trans. Energy Convers.*, vol. 37, no. 4, pp. 2837–2850, Dec. 2022, doi: 10.1109/TEC.2022.3203770.

[9] A. Ordoño, E. Unamuno, J. A. Barrena, and J. Paniagua Amillano, "Interlinking converters and their contribution to primary regulation: A review," *Int. J. Elect. Power Energy Syst.*, vol. 111, pp. 44–57, Apr. 2019, doi: 10.1016/j.ijepes.2019.03.057.

[10] M. Paolone et al., "Fundamentals of power systems modelling in the presence of converter-interfaced generation," *Electric Power Syst. Res.*, vol. 189, 2020, Art. no. 106811, doi: 10.1016/j.epsr.2020.106811. [Online]. Available: https://www.sciencedirect.com/science/article/pii/S037877962030482X

[11] J. Rocabert, A. Luna, F. Blaabjerg, and P. Rodríguez, "Control of power converters in AC microgrids," *IEEE Trans. Power Electron.*, vol. 27, no. 11, pp. 4734–4749, Nov. 2012, doi: 10.1109/TPEL.2012.2199334.

[12] T. L. Vandoorn, B. Renders, L. Degroote, B. Meersman, and L. Vandevelde, "Active load control in islanded microgrids based on the grid voltage," *IEEE Trans. Smart Grid*, vol. 2, no. 1, pp. 139–151, Mar. 2011, doi: 10.1109/TSG.2010.2090911.

[13] H. Liu et al., "An enhanced dual droop control scheme for resilient active power sharing among paralleled two-stage converters," *IEEE Trans. Power Electron.*, vol. 32, no. 8, pp. 6091–6104, Aug. 2017, doi: 10.1109/TPEL.2016.2614324.

[14] J. Wang, C. Dong, C. Jin, P. Lin, and P. Wang, "Distributed uniform control for parallel bidirectional interlinking converters for resilient operation of hybrid AC/DC microgrid," *IEEE Trans. Sustain. Energy*, vol. 13, no. 1, pp. 3–13, Jan. 2022, doi: 10.1109/TSTE.2021.3095085.

[15] X. Li et al., "Flexible interlinking and coordinated power control of multiple DC microgrids clusters," *IEEE Trans. Sustain. Energy*, vol. 9, no. 2, pp. 904–915, Apr. 2018, doi: 10.1109/TSTE.2017.2765681.

[16] H. Hu, M. Zhu, X. Li, and X. Cai, "Virtual DC machine based islanding detection method in DC distribution system and stability enhancement," in *Proc. 46th Annu. Conf. IEEE Ind. Electron. Soc.*, 2020, pp. 3277–3282, doi: 10.1109/IECON43393.2020.9254591.

[17] D. Huang, S. Fan, and B. Fan, "Virtual DC generator control strategy for load DC–DC converter," in *Proc. Int. Symp. Comput. Informat.*, 2015, pp. 1359–1368, doi: 10.2991/isci-15.2015.181.

[18] C. Gómez-Aleixandre, A. Navarro-Rodríguez, G. Villa, C. Blanco, and P. García, "Adaptive droop controller for a hybrid 375 Vdc/48 Vdc/400 vac AC/DC microgrid," *IEEE Trans. Ind. Appl.*, vol. 58, no. 4, pp. 5104–5116, Jul./Aug. 2022, doi: 10.1109/TIA.2022.3176597.

[19] A. Navarro-Rodríguez, P. García, R. Georgious, and J. García, "Adaptive active power sharing techniques for DC and AC voltage control in a hybrid DC/AC microgrid," *IEEE Trans. Ind. Appl.*, vol. 55, no. 2, pp. 1106–1116, Mar./Apr. 2019, doi: 10.1109/TIA.2018.2873543.

[20] T. K. Vrana, J. Beerten, R. Belmans, and O. B. Fosso, "A classification of DC node voltage control methods for HVDC grids," *Electric Power Syst. Res.*, vol. 103, pp. 137–144, 2013, doi: 10.1016/j.epsr.2013.05.001. [Online]. Available: https://www.sciencedirect.com/science/article/pii/S0378779613001193

Carlos Gómez-Aleixandre (Member, IEEE) received the B.Sc. degree in electrical engineering and the B.Sc. degree in industrial electronic and automatic engineering from the University of Oviedo, Gijón, Spain, in 2015 and 2018, respectively, and the M.Sc. degree in sustainable transportation and electrical power systems from the University of Oviedo, University of Nottingham, Nottingham, U.K., Sapienza Università di Roma, Rome, Italy, and Instituto Superior de Engenharia de Coimbra, Coimbra, Portugal, in 2017. He is currently working toward the Ph.D. degree in electrical engineering with the LEMUR Research Team, University of Oviedo.

He has coauthored four IEEE journals and seven IEEE international conference papers. His research interests include microgrids, coordinated control, and modeling and control of islanded and grid-connected converters.

Mr. Gómez-Aleixandre was the recipient of a Spanish Predoctoral Grant for the formation in university teaching (Formación de Profesorado Universitario) in 2017.

Ángel Navarro-Rodríguez (Member, IEEE) received the B.Sc. degree in telecommunications engineering with honours from the University of Castilla La-Mancha, Ciudad Real, Spain, in 2012, the M.Sc. degree in electrical energy conversion and power systems, and the Ph.D. degree (*Cum Laude*) in energy and process control from the University of Oviedo, Oviedo, Spain, in July 2014 and June 2019, respectively, granted by the government of Principado de Asturias.

He has been an Assistant Professor with the Department of Electrical, Electronics, Communications, and Systems Engineering, University of Oviedo since October 2019. In 2016–2017, he was a Visitor Researcher with the PEMC Research Group, The University of Nottingham, Nottingham, U.K. In 2022, he was a Visitor Researcher with the Chair of Power Electronics in the University of Kiel, Kiel, Germany. He has authored or coauthored 14 IEEE journals and more than 20 IEEE conferences. He has been a part of the LEMUR Research Group, University of Oviedo since July 2014 and his current research interests include microgrids control and modelling, grid-tied converters, energy storage systems, control systems applied to electrical energy conversion, sustainable transportation and electric traction, power quality, renewable energies integration, grid modernization, and smart grids.

Dr. Navarro-Rodríguez was the recipient of the Outstanding Young EPE Member Award in 2018 and the University of Oviedo Outstanding Ph.D. Thesis Award in 2020.

Marius Langwasser (Member, IEEE) received the M.Sc. and Ph.D. degrees from Kiel University, Kiel, Germany, in 2016 and 2021, respectively.

He is currently a Senior Postdoctoral Scientific Staff Member and the Leader of the Group "Electric Grids," Chair of Power Electronics, Kiel University. He is the Principal Investigator and project leader for the Kopernikus-project ENSURE and responsible for the Marie Sklodowska-Curie Research Actions Wingrid and SMARTGYsum. His research interests include control and protection of meshed and hybrid grids, dynamically reconfigurable grids and grid service provision with high-voltage direct current (HVdc) systems and smart transformers.

Pablo García (Senior Member, IEEE) was born in Luanco, Asturias, Spain. He received the M.S. and Ph.D. degrees in electrical engineering from the University of Oviedo, Gijon, Spain, in 2001 and 2006, respectively,

In 2004, he was a Visiting Scholar with the University of Wisconsin-Madison, Madison, WI, USA. In 2013, he was a Visiting Scholar with The University of Nottingham, Nottingham, U.K. He is currently a Full Professor with the Department of Electrical, Electronics, Communications and Systems Engineering, University of Oviedo. Since 2022, he has been with the Spanish Research Agency as the Manager for international projects in the Energy and Transport division area. He is the coauthor of more than 40 journal papers and more than 80 international conference papers. His research interest includes control of grid-tied power converters for distributed resources integration and particularly for the control of grid-tied battery energy storage systems, parameter estimation, optimization of distributed resources, and digital signal processing for real-time embedded systems.

Dr. García was the recipient of the 2005 IEEE TRANSACTIONS ON INDUSTRY APPLICATIONS, Third Place Prize Paper Award, three IEEE Industry Applications Society Conference prize paper awards in 2006, 2010, and 2016, respectively and one EPE Conference Award in 2018 and was also a fellowship for the national research and training program by the Ministry of Science and Technology in Spain, from 2002 to 2006. He is a member of the LEMUR research group. He has been the Principal Investigator of 50 projects with companies, one European H2020, and four national funded projects. He is the cofounder of the ENFASYS startup, focused on the development of solutions for the integration of energy storage in distribution and generation applications.

Marco Liserre (Fellow, IEEE) received the M.Sc. and Ph.D. degrees in electrical engineering from the Politecnico di Bari, Bari, Italy, in 1998 and 2002, respectively.

He has been Associate Professor at the Politecnico di Bari and, since 2012, Professor of Reliable Power Electronics at Aalborg University (Denmark), Aalborg, Denmark. Since 2013, he has been a Full Professor and holds the Chair of Power Electronics with the University of Kiel, Kiel, Germany. He has been offered and declined professorships with several universities. He has authored or coauthored more than 700 technical papers (1/3 of them in international refereed journals), one book, and five granted patents. These works have received more than 50,000 citations.

Dr. Liserre was selected as a Highly Cited Researcher in the field of Engineering (Clarivate Web of Science) from 2014 to 2021. Several of his students (M.Sc., Ph.D., and postdocs) are in leading positions in industry and universities worldwide. In 2023, he joined the Fraunhofer ISIT on a part-time basis as deputy Director and Director of the new division "Electronic Energy Systems," as well as of the Kiel branch of the Fraunhofer ISIT. He is a member of IAS, PELS, PES, and IES. He has served all these societies in various capacities. In PELS, he is Co-Editor of the *IEEE Open Access Journal in Power Electronics* and Technical Committee Chairman of the Committee on Electronic Power Grid Systems. He has Co-Chaired several IEEE conferences being several times Chairman. He was the recipient of 16 awards from IEEE, PCIM, and EPE-PEMC, including the prestigious 2018 IEEE-IES Mittelmann Achievement Award and the 2023 IEEE-PELS R. David Middlebrook Achievement Award. In 2023, he was also the recipient of title of "Ufficiale" by the President of the Italian Republic. In 2025, he will be Chairman of Powertech 2025 in Kiel.